Available online at www.sciencedirect.com
ScienceDirect
Journal of African Earth Sciences 46 (2006) 281–299
Journal of African Earth Sciences
www.elsevier.com/locate/jafrearsci

An extended field of crater-shaped structures in the Gilf Kebir region, Egypt: Observations and hypotheses about their origin

Philippe Paillou [a,*], Bruno Reynard [b], Jean-Marie Malézieux [c], Jean Dejax [d], Essam Heggy [e,f], Pierre Rochette [g], Wolf Uwe Reimold [h,i], Patrick Michel [j], David Baratoux [k], Philippe Razin [l], Jean-Paul Colin [m]

[a] *Observatoire Aquitain des Sciences de l'Univers, UMR 5804, 2, rue de l'Observatoire, BP 89, 33270 Floirac, France*
[b] *Ecole Normale Supérieure, UMR 5570, Lyon, France*
[c] *Université Bordeaux 3, UMR 5804, Pessac, France*
[d] *Muséum National d'Histoire Naturelle, UMR 5143, Paris, France*
[e] *Lunar and Planetary Institute, Houston, USA*
[f] *Cairo University, Department of Astronomy, Giza, Egypt*
[g] *Université d'Aix-Marseille 3, CEREGE, Aix en Provence, France*
[h] *University of the Witwatersrand, School of Geosciences, Johannesburg, South Africa*
[i] *Humboldt University, Museum für Naturkunde, Berlin, Germany*
[j] *Observatoire de la Côte d'Azur, UMR 6202, Nice, France*
[k] *Observatoire Midi-Pyrénées, UMR 5562, Toulouse, France*
[l] *Université Bordeaux 3, Institut EGID, Pessac, France*
[m] *3 Impasse des Biroulayres, 33610 Cestas, France*

Received 9 December 2005; received in revised form 11 April 2006; accepted 31 May 2006
Available online 28 July 2006

Abstract

Using satellite imagery, we detected more than 1300 small crater-like structures distributed over an area of 40,000 km^2 in the Western Egyptian Desert, close to the Gilf Kebir plateau. Sixty-two of them were visited in the field, and morphological observations, rock samples and ground-penetrating radar data were obtained. After presenting our fieldwork results, we discuss two hypotheses for their origin: hydrothermal vent complexes and meteorite impacts. At present, none of them fully satisfies the available observations.
© 2006 Elsevier Ltd. All rights reserved.

1. Introduction

Using satellite imagery, we detected more than one thousand intriguing structures in the Western Egyptian desert. They are crater-shaped depressions, with often circular or elliptical rims, that sometimes can also be more irregular or polygonal. These structures appear often in the form of clusters, some of them overlapping, and small rimmed depressions are also sometimes embedded in larger ones. The structures are more or less complete, appearing in various state of erosion, and they are distributed over an area of more than 40,000 km^2 East of the Gilf Kebir plateau. Results of a first field study realized in February 2004 led us to speculate on a possible impact origin for some of these structures (Paillou et al., 2004). Since then, analysis of new satellite imagery of the region and fieldwork performed in December 2004 considerably extended the field area and the number of structures, making the impact origin even less plausible. An endogenic phenomenon, such as hydrothermal venting capable of creating numerous craters over a large area (Svensen et al., 2003), could provide an alternative explanation for the observed structures, although some observations do not agree with this hypothesis either.

* Corresponding author. Tel.: +33 557 776 126; fax: +33 557 776 110.
E-mail address: paillou@obs.u-bordeaux1.fr (P. Paillou).

1464-343X/$ - see front matter © 2006 Elsevier Ltd. All rights reserved.
doi:10.1016/j.jafrearsci.2006.05.006

Crater-shaped structures can be tracked with the aid of radar imaging from space, which allows mapping of subsurface geology in arid regions with high spatial resolution. In particular, structures filled and partially hidden by aeolian deposits may not be recognized using classical optical imaging systems, but a rougher crater rim can appear as a radar-bright feature that assists detection (McHone et al., 2002). Using such techniques, we identified a large number of crater-like structures in a radar mosaic of the Eastern Sahara composed of JERS-1 satellite scenes. This dataset has already permitted the discovery of a doublet crater feature in southeast Libya, of possible meteoritic origin (Paillou et al., 2003a; Koeberl, 2004). We initially studied a region located 115 km East of the Gilf Kebir plateau in the Western Egyptian Desert, where we observed tens of small circular features in radar images, with diameters between 100 m and 2 km, over a 4500 km^2 region between latitudes 23°10′N–23°40′N and longitudes 26°50′E–27°35′E. Initial fieldwork in February 2004 allowed us to visit 13 structures with diameters from 20 to 1300 m, of near-circular morphology, with variable low (a few meters) to high (more than 80 m) rims. The height of the rims of the largest structures and the frequent presence of small ones indicate that these structures are either quite young or were preserved from erosion by post-formational sedimentary deposits. Abundant breccias were observed along the rims of all structures, forming tens of centimeter to meter thick beds, sometimes covered with paleo-soils, and features resembling shatter cones were found along the edges of several structures. Most of the rocks sampled on site contain quartz grains with sub-planar micro-deformations, reminiscent of PFs known from shock deformed quartz. This led us to speculate on an impact origin for these structures (Paillou et al., 2004).

Another field trip in December 2004 allowed us to visit 49 additional structures, which extend the initial study area both to the North and the West. In addition to field observations, we performed ground-penetrating radar (GPR) soundings on several structures in order to investigate their internal geometry under aeolian deposits. Fossils (ostracodes and wood) discovered in the sediments filling one structure are described: together with the observation of basalt dykes intruding some structures, they provide some constraints on their formation age. Based on our observations, we discuss two possible origins of the structures, hydrothermal vent complexes and meteorite impacts, and we try to estimate their age of formation.

2. Satellite image analysis

2.1. Site selection for field work

With its subsurface imaging capabilities, orbital synthetic aperture radar is a unique tool for mapping geology in arid areas (Paillou et al., 2003b). Nevertheless, complementary higher-resolution visible imagery is useful for navigation in the field, once a region of interest has been identified. Having initially located a possible crater field in JERS-1 radar images (Paillou et al., 2004), we then acquired high-resolution (10 m) satellite images in optical wavelengths provided by the French SPOT 4 satellite. Our region of interest, 225×215 km in extent, is located in Southwest Egypt, in the vicinity of the Gilf Kebir plateau (Fig. 1). We assembled a 10-m-resolution mosaic of this area using sixteen SPOT 4 scenes (Fig. 2). As most studied structures are exposed above the surficial sand sheet, they can be seen on such high-resolution satellite data. We then manually processed the SPOT 4 mosaic in order to mark all crater-shaped structures: 1312 such structures were identified this way, occurring over more than 40,000 km^2 (cf. red circles in Fig. 2). The SPOT 4 mosaic was then used to define candidate sites for ground exploration: the December 2004 mission allowed us to explore the new sites 1, 2a, and 2b indicated on Fig. 2. Sites 3a and 3b had already been studied during the first field mission in February 2004, but we revisited them in December 2004.

East of the Gilf Kebir plateau, the exposed rocks belong mainly to the Sabaya Formation of Middle Cretaceous (Albian to Cenomanian) age, consisting of medium- to coarse-grained fluvial sandstone interbedded with muddy paleo-soil horizons (Klitzsch et al., 1987). The area is partially covered with Quaternary aeolian sand deposits. The southern limit of the studied region also exposes outcrops of the Aptian Abu Ballas Formation, consisting of shallow near-shore marine to coastal siltstone and fine-grained sandstone. Issawi (1978) provided information regarding the brecciation, ferruginisation, and deformation of the bedding in this region. The Gilf Kebir, located in the extreme southwestern region of Egypt close to the Sudanese and Libyan borders, is a large 1100-m-high plateau made up of late Jurassic to Cretaceous clastic sediments. The upper part of the Gilf Kebir plateau sequence is composed of Cretaceous strata equivalent to the Sabaya and Maghrabi Formations (Cenomanian, mainly paleo-soils and fluvial sandstone). During the upper Cretaceous, strike-slip movement along the present-day Red Sea axis converted the Pan African East-West shear planes into normal faults, with alkali-olivine basaltic volcanism accompanying this tectonic phase (Klitzsch and Schandelmeier, 1990). A few crater structures have already been observed in the past in this region. El-Baz (1981, 1982) noticed crater forms in the Uweinat region, some of which are now established as volcanic features (Barakat, 1994). Several "circular features" are mentioned on the geological map of Klitzsch et al. (1987), with a few small Tertiary alkali-olivine basalt outcrops reported in the northwestern part of the region. A couple of other circular features, the so-called "Clayton craters", were reported in the southern part of the Gilf Kebir; they are considered to be of volcanic origin (Clayton, 1933; Sandford, 1935).

Extracts of the SPOT 4 mosaic at 10-m resolution are presented in Figs. 3–8. Figs. 3 and 4 show sites 3b and 3a, respectively; these two sites were studied during the February 2004 expedition, when 13 structures were visited

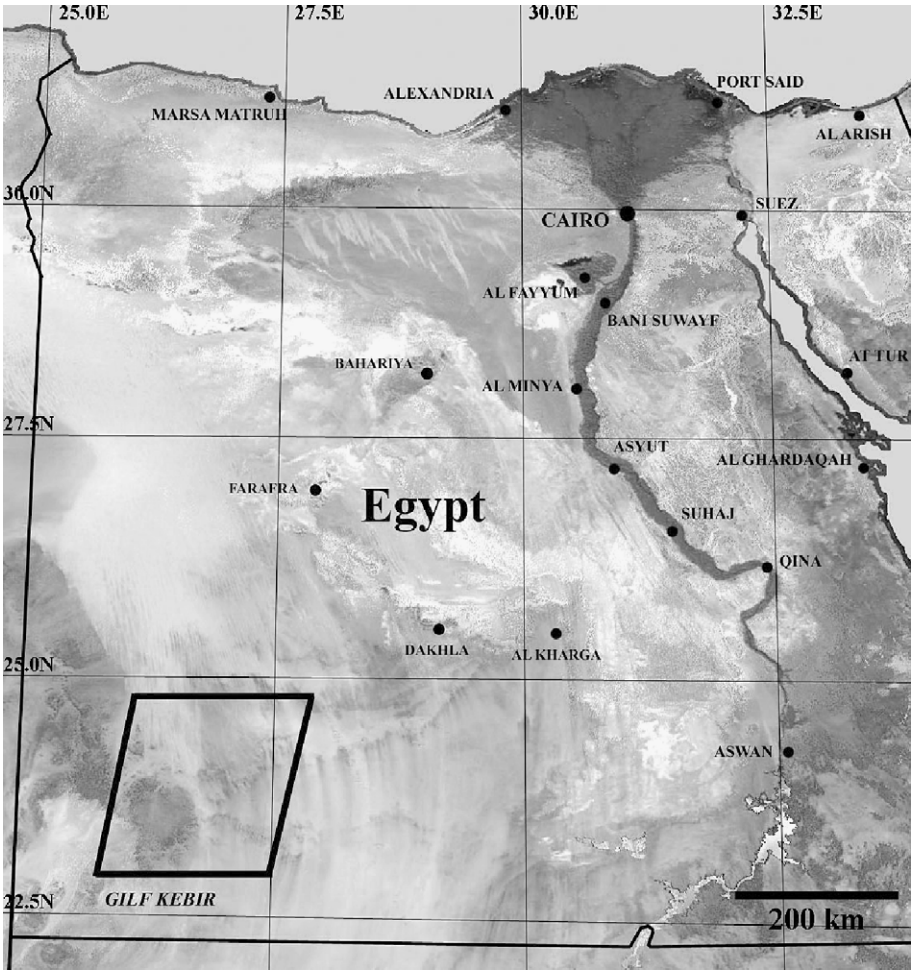

Fig. 1. SPOT Vegetation image of Egypt with the Gilf Kebir study region indicated (lower left, 225 × 215 km in size).

(GKCF01 to GKCF13) (cf. Paillou et al., 2004). Fig. 5 presents the northernmost site we could visit in December 2004; it shows a major circular structure of 2100 m diameter, possibly presenting a double ring (GKCF59). Figs. 6 and 7 show, respectively, the northern and southern parts of site 2a, which contains a high density of crater-shaped structures: we visited more than 35 of them, with diameters between 10 m and 1300 m. Finally, a site located on the northeastern part of the Gilf Kebir plateau, where two quasi-circular structures are crossed by small non-permanent rivers (wadis), was visited (Fig. 8).

2.2. Distribution and morphology of the structures

The spatial distribution of the 1312 structures in our study region, identified in SPOT 4 satellite images, is shown in Fig. 9. Three main clusters are clearly distinguished. The southwestern cluster comprises approximately 190 structures and is located on the Gilf Kebir plateau. This cluster contains site 1 (cf. Fig. 8). The southeastern cluster contains about 560 structures, and is the location of sites 3a (cf. Fig. 4) and 3b (cf. Fig. 3). The northern cluster also contains about 560 structures and is the location of sites 2a (cf. Figs. 6 and 7) and 2b (cf. Fig. 5). It should be noted that the map presented in Fig. 9 is incomplete: differential erosion may have removed structures in some places, and large sand dunes certainly hide a significant number of them (in particular, the northwestern part of the region is covered by N-S trending sand dunes of the Great Sand Sea).

A great number of structures are not perfectly circular (cf. Fig. 4 for instance), some presenting a polygonal shape, possibly the result of several structures being imbricate. However, their general shape is more likely a circle than an ellipse, and the angular forms of some structures could also result from erosion and possibly tectonic overprint. Out of a total of 1312 structures identified in SPOT 4 images, 465 are well-formed circular features and 249 present a clear elliptical shape. About 70% of the elliptical structures are oriented along 36°N and the remaining 30% are oriented along 335°N. These two directions seemingly correspond to the orientations of the main faults reported on the geological map of Klitzsch et al. (1987), indicating that some structures might have been deformed by tectonic events that took place during the Eocene (Alpine Orogeny) and Oligocene (rifting of the Red Sea) (Meshref, 1990).

The size distribution for all these 1312 crater-like structures is presented in Fig. 10 (left). We can observe that it

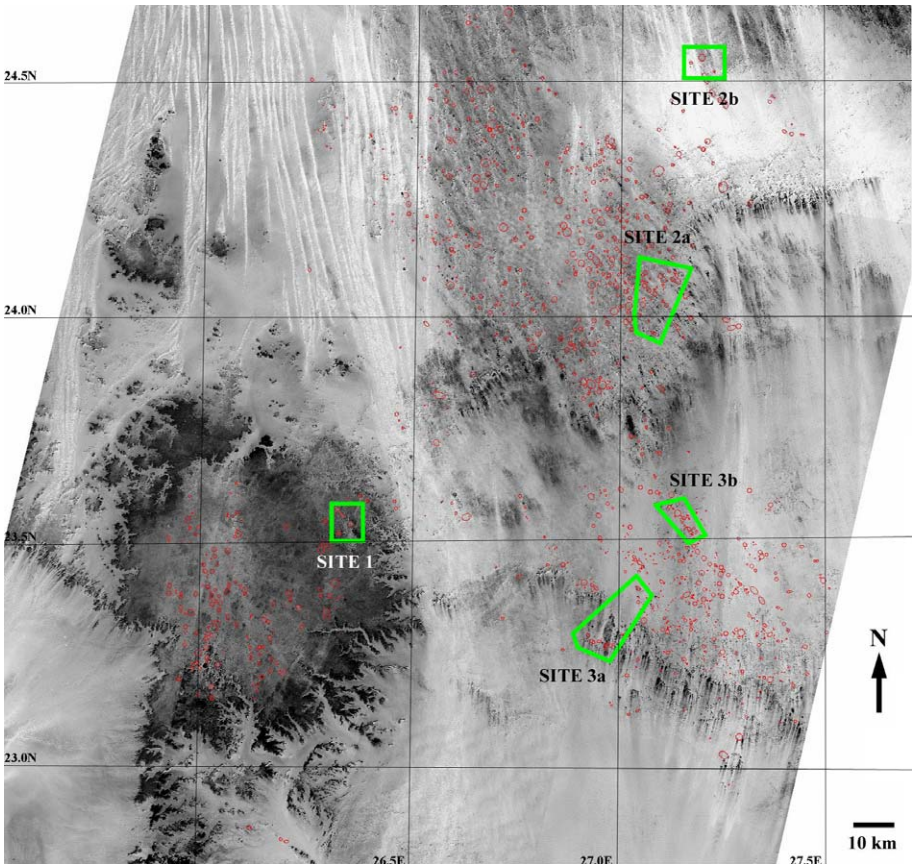

Fig. 2. Mosaic of 16 SPOT 4 scenes of the study region covering 225 × 215 km (data from SPOT/ISIS/CNES program). The 1312 crater structures are indicated as red circles, whereas field study areas are in green. The Gilf Kebir plateau is at the lower left.

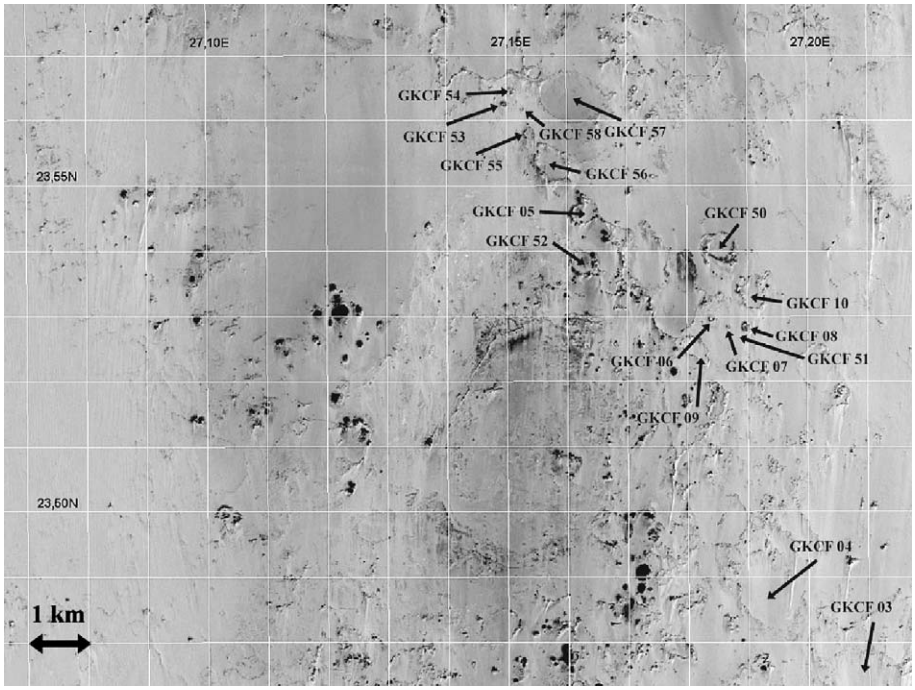

Fig. 3. SPOT 4 image of study site 3b (10 m resolution). Structures visited during fieldwork are marked GKCF xx (cf. Table 1).

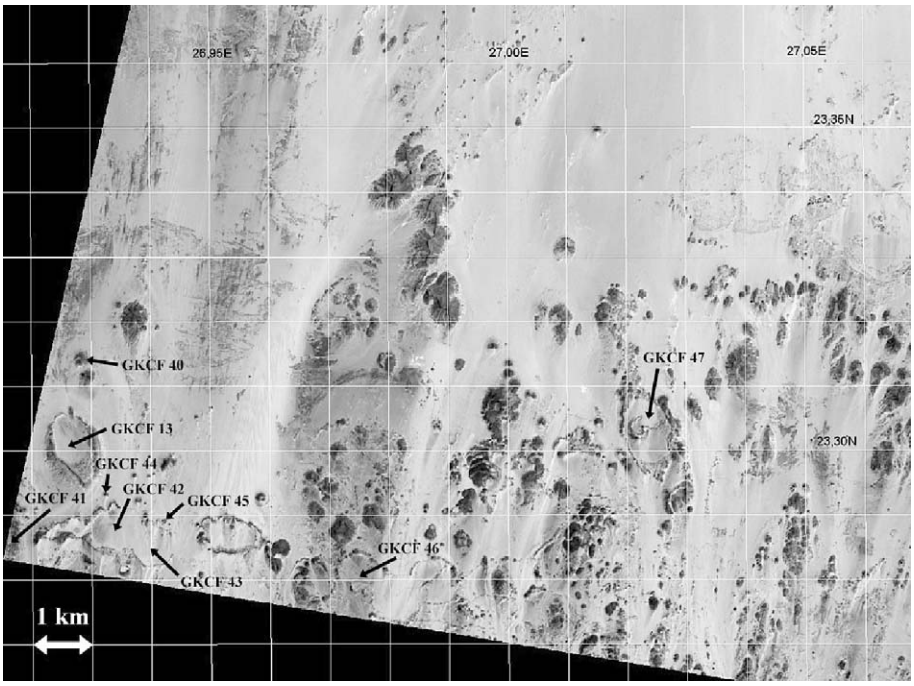

Fig. 4. SPOT 4 image of study site 3a (10 m resolution). Structures visited during fieldwork are marked GKCF xx (cf. Table 1).

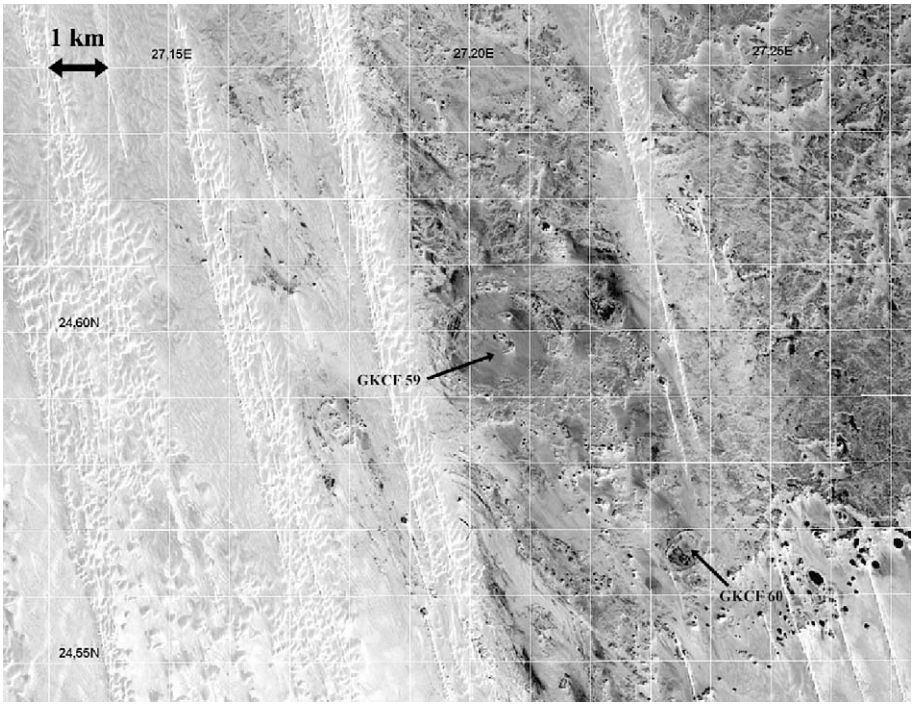

Fig. 5. SPOT 4 image of study site 2b (10 m resolution). Structures visited during fieldwork are marked GKCF xx (cf. Table 1).

presents an exponential decrease. The diameter of the smallest structure that could be detected in the SPOT 4 images is 50 m (the image resolution being 10 m): this explains why the number of detected structures decreases towards small diameters. In fact, several structures with a diameter smaller than 50 m could be observed in the field, but they are generally difficult to detect because of lower rims, which often barely protrude above the younger aeolian deposits. We suspect that lots of similar small structures are still hidden underneath the Quaternary sand

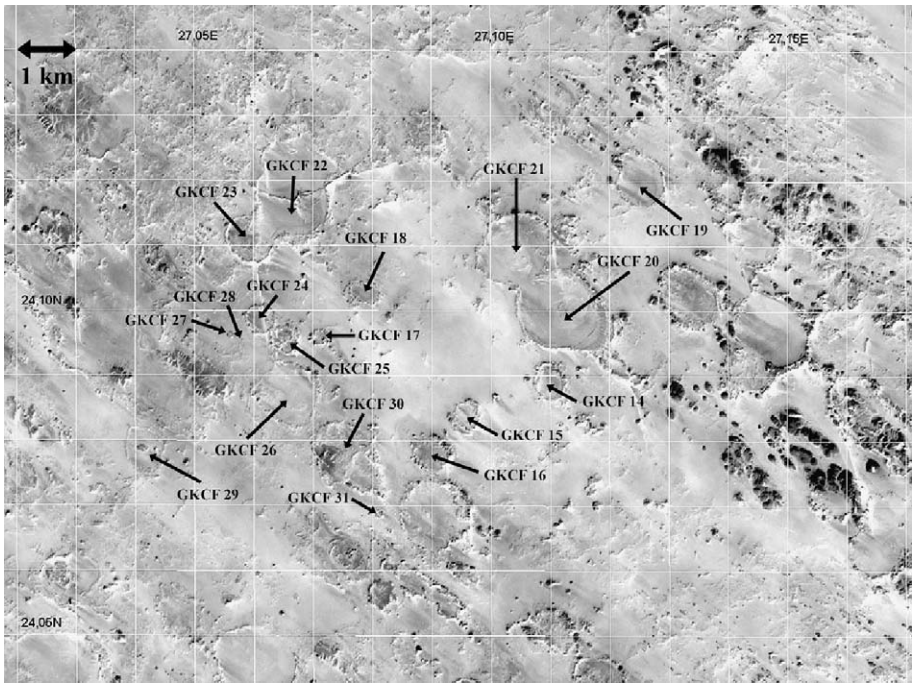

Fig. 6. SPOT 4 image of study site 2a north (10 m resolution). Structures visited during fieldwork are marked GKCF xx (cf. Table 1).

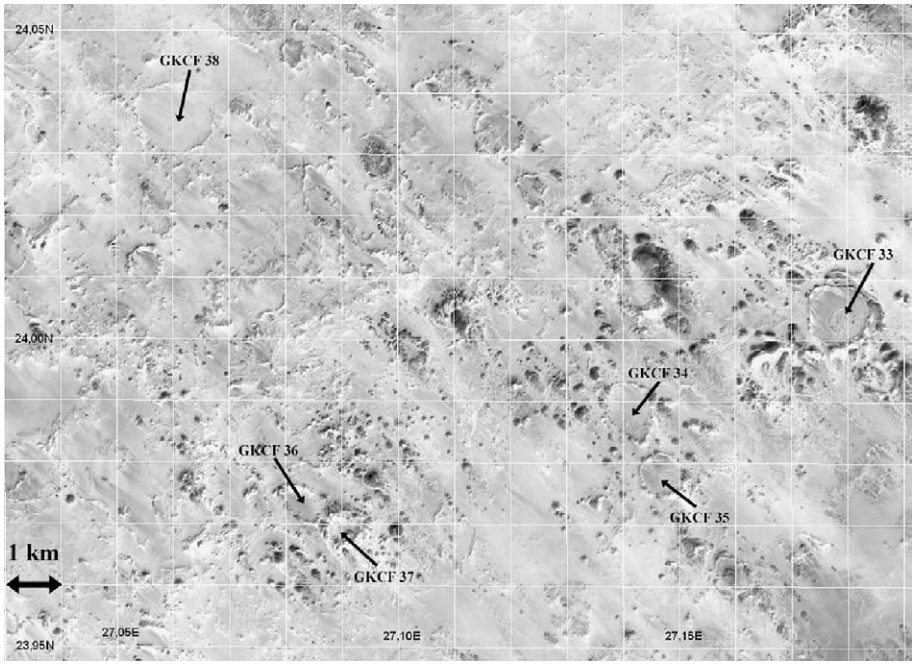

Fig. 7. SPOT 4 image of study site 2a south (10 m resolution). Structures visited during fieldwork are marked GKCF xx (cf. Table 1).

sheet. The largest structure found on satellite images has a diameter of 2500 m. The mean diameter for all structures is around 520 m, with a standard deviation of 450 m, whereas most of the structures have a diameter of the order of 150 m. In the dataset of 1312 structures, 42 are doublets—two well-defined and connected structures (see for instance GKCF20 and GKCF21 in Fig. 6), and the mean distance between two neighboring structures is 1330 m.

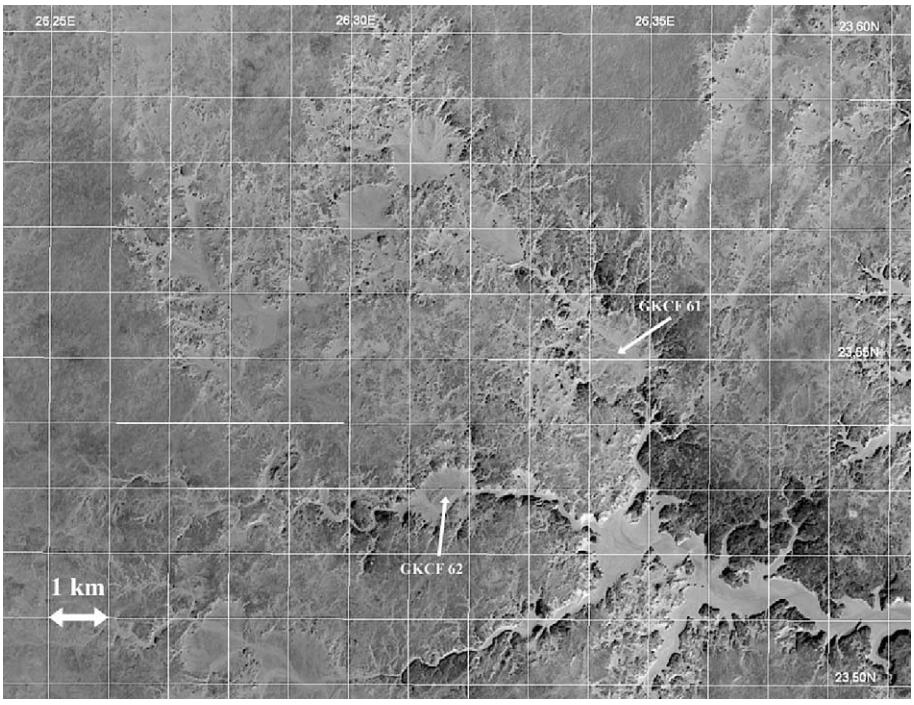

Fig. 8. SPOT 4 image of study site 1 (10 m resolution). Structures visited during fieldwork are marked GKCF xx (cf. Table 1).

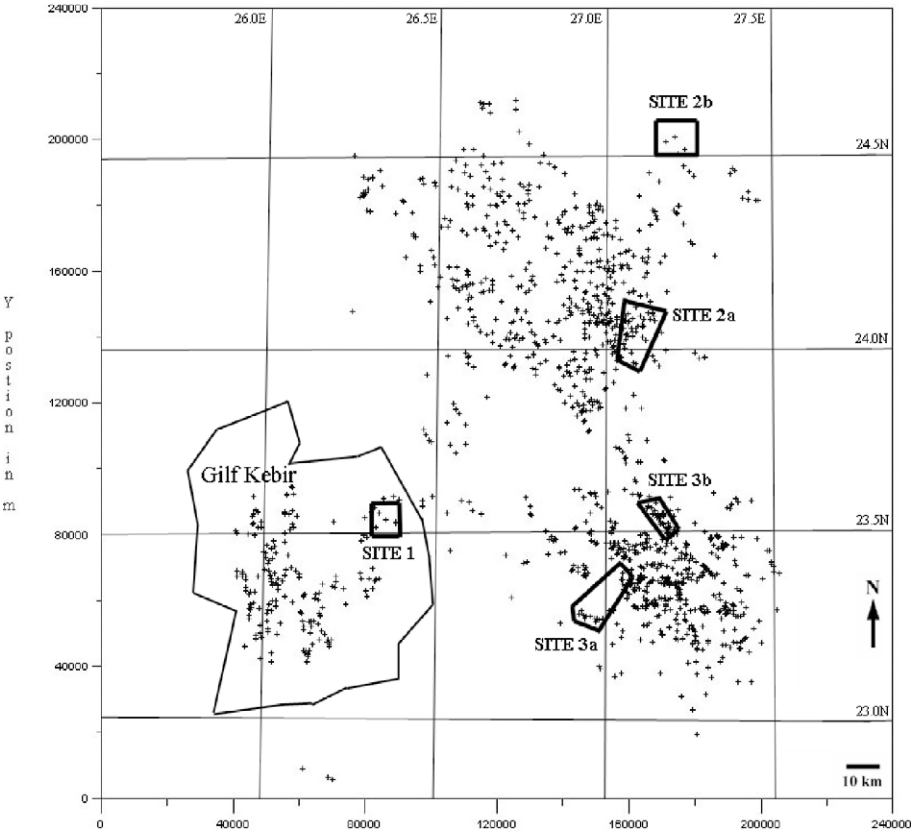

Fig. 9. Location map of the 1312 crater-shaped structures detected in satellite images (scales are shifted UTM coordinates).

Fig. 10 (right) also shows the elevation distribution of the structures. We used topographic information extracted from SRTM (Shuttle Radar Topography Mission [http://srtm.usgs.gov/]) data to obtain the elevation of each of the 1312 structures. The histogram in Fig. 10 (right) shows two main peaks: most of the structures are located at an

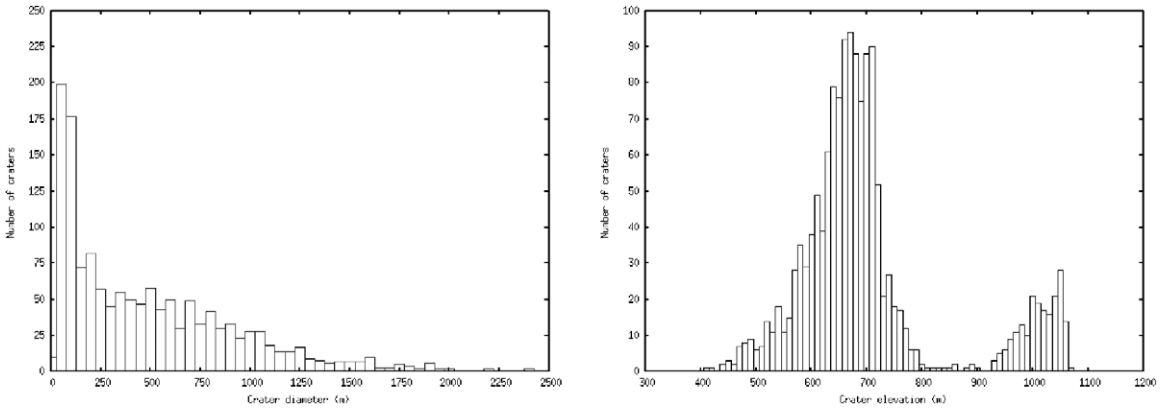

Fig. 10. Left: histogram of the distribution of the diameter of the 1312 structures (the *y*-axis is the number of structures in each class and the *x*-axis is the structure diameter in meters). Right: histogram of the distribution of the elevation of the 1312 structures (the *y*-axis is the number of structures in each class and the *x*-axis is the structure elevation in meters).

average elevation of 680 m on the Sabaya Formation, while the remaining ones are located higher, around 1000 m in elevation, on the Gilf Kebir plateau.

3. Results of field investigations

A summary of information related to the 62 structures visited in February and December 2004 is presented in Table 1. Their diameters range from 10 m to 2120 m. Except for a couple of small structures covered by the Quaternary sand sheet, most of them present well-defined rims, with heights ranging from a couple of meters to more than 80 m for GKCF13 (Fig. 11). Most structures are more or less filled with Quaternary aeolian deposits, their center being in general higher than the surroundings; it seems that erosion removed sedimentary deposits around the structures and exhumed them as peaks in the landscape (see for example GKCF13 and Fig. 11 and GKCF08 in Fig. 12). The height/diameter ratio of the visited structures ranges from 0.05 to 0.1. The smallest structures (diameter less than 30 m) have very steep inward-dipping (up to 60°) rims. Rims are made of tilted sandstone layers of the Sabaya Formation covered by breccia, sometimes also covered by paleo-soils on their inner part (cf. Table 1) as illustrated in Fig. 13. Most of the rim sections are impregnated by iron oxide, probably a mineralization result of fluid circulations that also produced ferruginous sandstone formations in the region (the so-called Black Hills). In a few structures where outcrops extend within the central zone, we could see the circular inward-dipping strata change progressively into either sub-horizontal deposits or chaotically oriented disrupted strata. Some structures are cross-cut by basalt dykes, indicating that magmatism took place after their formation. Since basalts in the region are of Lutetian age (the age of 59 Ma initially proposed by Klitzsch et al. (1987) was later refined to 46 Ma by Meneisy (1990) on the basis of K/Ar data), we can conclude that the structures certainly formed before this time. All these structures seem to have been produced by the same process: except for a few on the Gilf Kebir plateau (cf. Fig. 8), they all present a similar morphology on both satellite images and in the field. Clearly, more fieldwork is needed to describe the morphology of these structures in detail and our observations are still far from complete: only 62 crater-like structures were visited among more than 1300.

3.1. Shatter-cone-like features and breccias

Shatter-cone-like features were found along the rim of several structures (cf. Table 1). Although wind erosion of exposed rocks or silicified cone-in-cone structures can produce analogous features (Lugli et al., 2005), in some places the perceived apices seem to point towards the centers of the structures. However, this should be confirmed by further measurements in the field, and we could not clearly observe the typical striation patterns of shatter cones (Sagy et al., 2004). Fig. 14 shows various shatter-cone-like features found in the field. Some of them seem to present conical patterns with "horsetail" markings (Roach et al., 1993), which are typical of impact shock waves propagating into rocks, corresponding to a 1–10 GPa pressure range (Sagy et al., 2002; Baratoux and Melosh, 2003; Nicolaysen and Reimold, 1999). However, the role of aeolian erosion and deflation is ubiquitous in the morphology of the Western Desert of Egypt, and some of the features presented in Fig. 14 look like ventifacts (the so-called pitted rocks) observed by McCauley et al. (1979). Also, wind erosion of exposed shatter cones could have led to the degradation of striations by sand abrasion. It would then be difficult to discriminate between pitted surfaces formed by wind erosion and curved fractures formed by a shock wave, having later been exposed to wind.

In few places, faulted zones with decimeter-sized tilted domains of originally cross-bedded sandstones were also observed, located outside but close to some structure rims. Such deformation might be related to tectonics. Abundant occurrences of breccias were observed along the rim of numerous structures (cf. Table 1), forming tens of

Table 1
List of the 62 structures we visited (GKCF: Gilf Kebir crater field, diameter: best fit circle diameter, SCLF: shatter-cone-like features, GPR: ground penetrating radar sounding, MD: sub-planar micro-deformations observed in sample)

Crater's name	Latitude N	Longitude E	Diameter (m)	Field observations	Sampling
GKCF01 (Ahmed)	23°14′37″	27°27′37″	630	Breccias, SCLF	Yes (MD)
GKCF02 (Nessim)	23°27′10″	27°19′18″	1000	Breccias, SCLF	Yes (MD)
GKCF03 (Gihan)	23°28′33″	27°12′26″	1300	Breccias, SCLF	Yes
GKCF04 (Bruno)	23°29′05″	27°11′12″	950	Breccias, tectonics	Yes
GKCF05 (Virginie)	23°32′42″	27°09′33″	450	Breccias, paleo-soils	No
GKCF06 (Roxane)	23°31′45″	27°11′05″	50	Breccias	Yes
GKCF07 (Nathan)	23°31′49″	27°10′57″	85	Breccias, GPR	Yes (MD)
GKCF08 (Sarah)	23°31′45″	27°11′17″	100	Breccias, GPR	Yes (MD)
GKCF09 (Jean-Marie)	23°31′13″	27°10′59″	710	Breccias	Yes (MD)
GKCF10 (Jean)	23°32′01″	27°11′20″	370	Breccias	No
GKCF11 (Aly)	23°28′15″	27°02′38″	1200	Breccias	Yes
GKCF12 (Ragab)	23°24′50″	26°57′04″	500	Breccias, SCLF	Yes (MD)
GKCF13 (Rahman)	23°18′23″	26°55′28″	950	Breccias, SCLF, paleo-soils, GPR	Yes (MD)
GKCF14 (Alaa)	24°05′20″	27°06′37″	560	Breccias, SCLF, paleo-soils, GPR	Yes
GKCF15 (Ahmed)	24°05′02″	27°05′45″	440	Breccias, GPR	No
GKCF16 (Said)	24°04′41″	27°05′24″	535	Breccias, SCLF	No
GKCF17 (Sacha)	24°05′46″	27°04′16″	230	Breccias, Basalt dyke	No
GKCF18 (Wahab)	24°06′10″	27°04′45″	360	Breccias, GPR	No
GKCF19 (Pierre)	24°07′13″	27°07′32″	825	Breccias	Yes
GKCF20 (Lucie)	24°06′00″	27°06′43″	1310	None	No
GKCF21 (Elise)	24°06′33″	27°06′17″	1220	Breccias, fossil wood, ostracodes, paleo-lake	Yes (MD)
GKCF22 (Frédéric)	24°06′58″	27°04′02″	1240	basalt dyke, paleo-soils	Yes
GKCF23 (Nathalie)	24°06′40″	27°03′35″	735	None	Yes (MD)
GKCF24 (Martin)	24°05′55″	27°03′40″	400	Breccias, basalt peak, paleo-soils	No
GKCF25 (Pauline)	24°05′44″	27°03′56″	380	Breccias	Yes (MD)
GKCF26 (Anne)	24°05′15″	27°03′59″	980	Breccias	No
GKCF27 (Inès)	24°05′47″	27°03′22″	100	Breccias	Yes (MD)
GKCF28 (Calin)	24°05′44″	27°03′29″	40	Breccias, GPR	No
GKCF29 (Monette)	24°04′41″	27°02′31″	650	Breccias, basalt dyke	Yes (MD)
GKCF30 (Pierre)	24°04′39″	27°04′35″	1020	Breccias, basalt dyke, paleo-soils	Yes (MD)
GKCF31 (Lucas)	24°04′08″	27°04′53″	110	Paleo-soils	No
GKCF32 (Chataigne)	24°05′43″	27°06′01″	10	None	No
GKCF33 (Alain)	24°00′51″	27°10′43″	1050	Breccias, SCLF, basalt dyke, paleo-soils	No
GKCF34 (Augustin)	23°59′55″	27°08′29″	880	Breccias, SCLF, paleo-soils	No
GKCF35 (Hadrien)	23°59′17″	27°08′50″	755	SCLF, paleo-soils	No
GKCF36 (Annick)	23°58′58″	27°05′00″	560	Breccias, SCLF	No
GKCF37 (Cécile)	23°58′46″	27°05′25″	530	Breccias, paleo-soils	No
GKCF38 (Pascale)	24°02′44″	27°03′40″	1150	Breccias	No
GKCF39 (Jérôme)	23°27′56″	26°32′15″	120	basalt peak, paleo-soils	Yes
GKCF40 (Raul)	23°18′50″	26°55′41″	80	Faults, tectonics	No
GKCF41 (Véronique)	23°17′15″	26°54′58″	30	None	No
GKCF42 (Michel)	23°17′16″	26°56′03″	775	Breccias, faults	No
GKCF43 (Pierrette)	23°17′07″	26°56′25″	720	Breccias, faults	No
GKCF44 (François)	23°17′36″	26°55′57″	50	None	No
GKCF45 (Alain)	23°17′21″	26°56′32″	55	Breccias	Yes
GKCF46 (Eric)	23°16′53″	26°58′30″	640	Breccias	No
GKCF47 (Marie)	23°18′09″	27°01′26″	1070	Breccias, basalt dyke	Yes
GKCF48 (Clara)	23°22′29″	27°02′58″	760	Breccias, basalt dyke	No
GKCF49 (Meryl)	23°22′21″	27°03′24″	60	Breccias	Yes
GKCF50 (Edmond)	23°32′26″	27°11′09″	550	Breccias, basalt dyke	No
GKCF51 (Coca)	23°31′37″	27°11′22″	10	GPR	No
GKCF52 (Philippe)	23°32′17″	27°09′46″	410	Breccias	No
GKCF53 (Hager)	23°33′45″	27°08′59″	80	Breccias	Yes
GKCF54 (Ossama)	23°33′52″	27°09′03″	90	None	No
GKCF55 (Magda)	23°33′29″	27°09′14″	180	Breccias	No
GKCF56 (Mohamed)	23°33′12″	27°09′28″	570	Breccias	No
GKCF57 (Essam)	23°33′48″	27°09′40″	900	Breccias, GPR	No
GKCF58 (Shereif)	23°33′43″	27°09′10″	50	Breccias	No
GKCF59 (Tarek)	24°35′53″	27°12′18″	2120	Double ring crater ?	No
GKCF60 (Catherine)	24°33′58″	27°14′08″	490	Multi-ring crater ?	No
GKCF61 (Christophe)	23°33′03″	26°20′42″	1450	On Gilf Kebir, GPR, paleo-soils, paleo-lake	No
GKCF62 (Luc)	23°31′44″	26°19′00″	980	On Gilf Kebir, paleo-lake	No

Fig. 11. The GKCF13 crater structure of 950 m diameter (view to the South). Rim elevation varies between 20 m and 80 m.

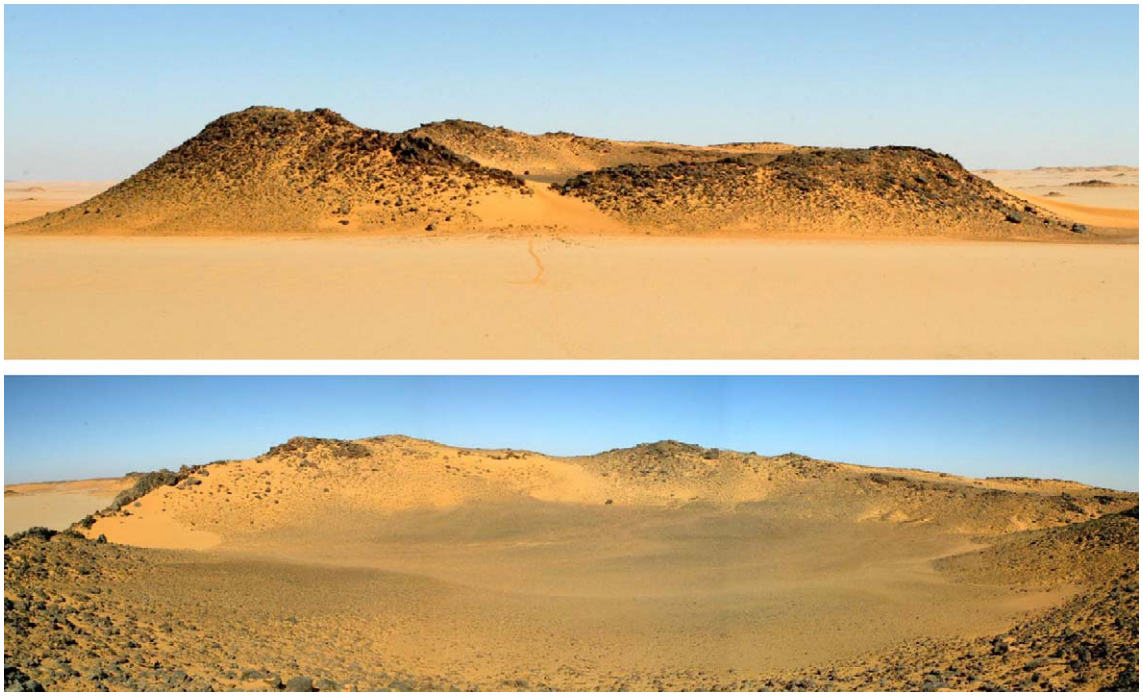

Fig. 12. The GKCF08 structure of 100 m diameter: view from outside to the East (top) and from inside to the North (bottom). Rims are about 8 m high.

centimeters to meter thick beds, sometimes interbedded with sandstones or covered by paleo-soils on their inner part. We could find both monomict and polymict breccia types that contain angular centimeter to meter sized clasts embedded in a fine-grained quartz-rich matrix, without indication of melting; some examples are shown in Fig. 15. We could only observe breccias in situ along the crater rims, as the inner and outer parts of the structures are covered with aeolian deposits. Such breccia formations can be produced by classical geological processes such as tectonics and rock falls. However, they do also occur in and around impact structures (Stöffler and Grieve, 1994), but at known small impact craters such as Aouelloul in Mauritania, Meteor crater in Arizona, or Henbury craters in Australia, no such breccias occur in the rims.

3.2. First petrographic results

We report here first results of optical microscopic analysis of thin sections of breccia and sandstone samples

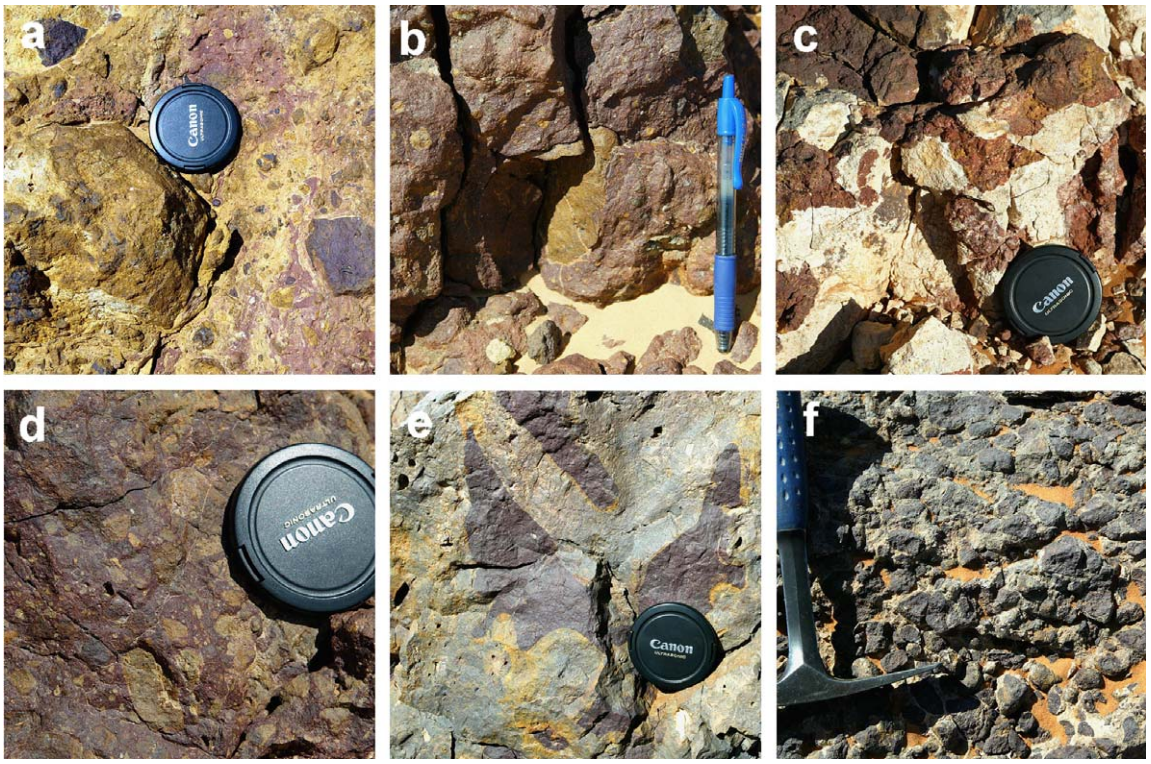

Fig. 13. Examples of various paleo-soil levels observed on the inner rim of several structures: (a) GKCF33, (b) GKCF14, (c) GKCF61, (d) GKCF37, (e) GKCF34, (f) GKCF13.

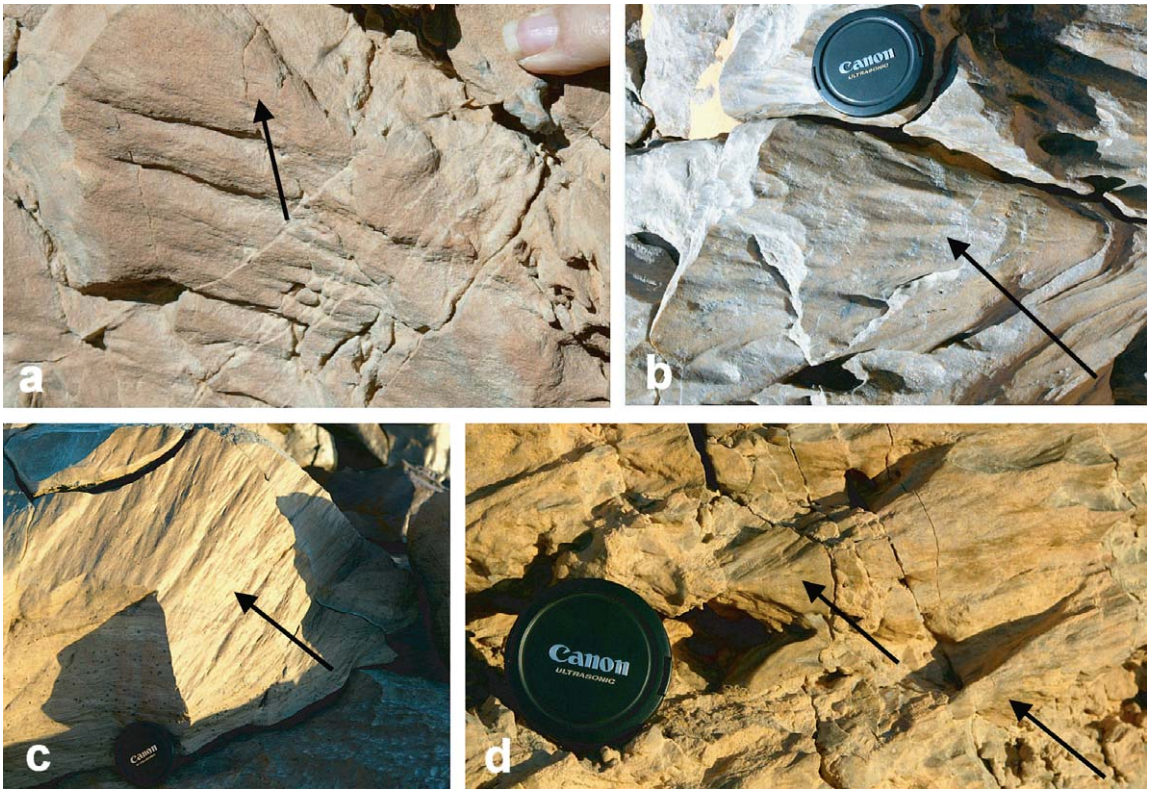

Fig. 14. Shatter-cone-like features observed along the rim of several structures: (a) GKCF13, (b) GKCF03, (c) GKCF02, (d) GKCF01. They can also be interpreted as ventifacts since all the surfaces present evidence of aeolian erosion. However, some curved surfaces show ambiguous striations (arrows) pointing to the center of the structure.

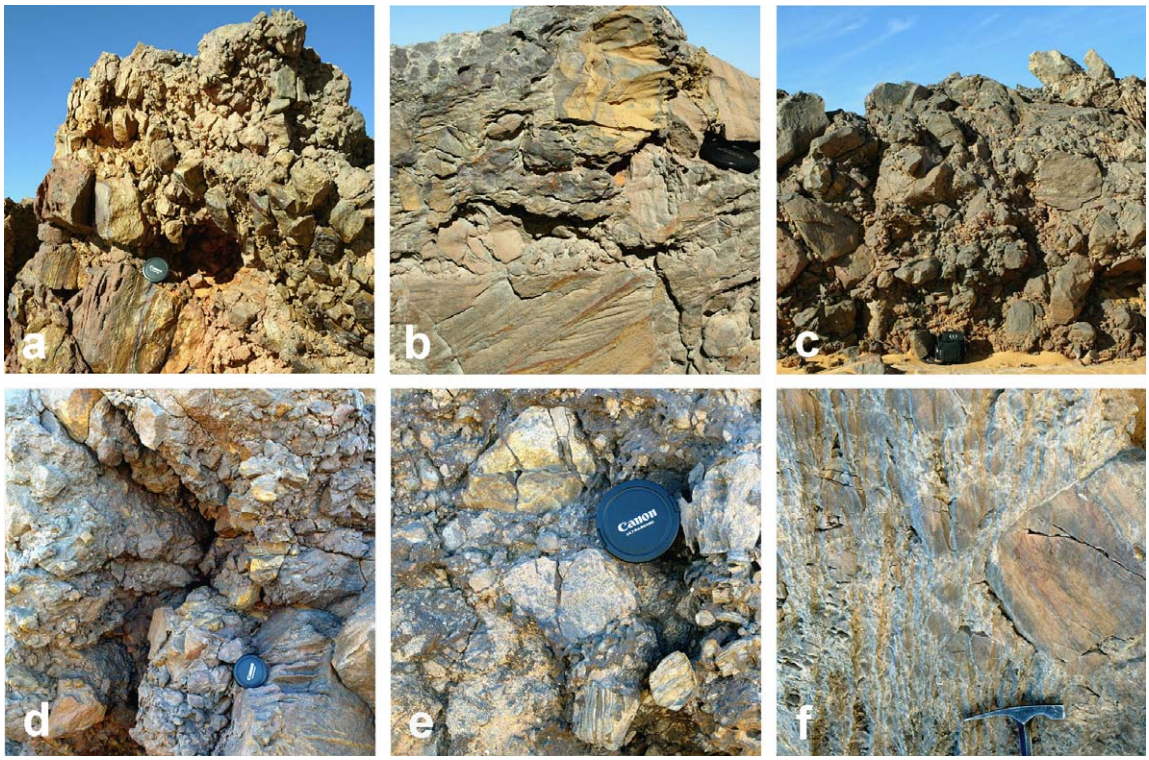

Fig. 15. Examples of breccias observed on the rim of several structures: (a) GKCF48, (b) GKCF13, (c) GKCF01, (d) GKCF02, (e) GKCF49, (f) GKCF13.

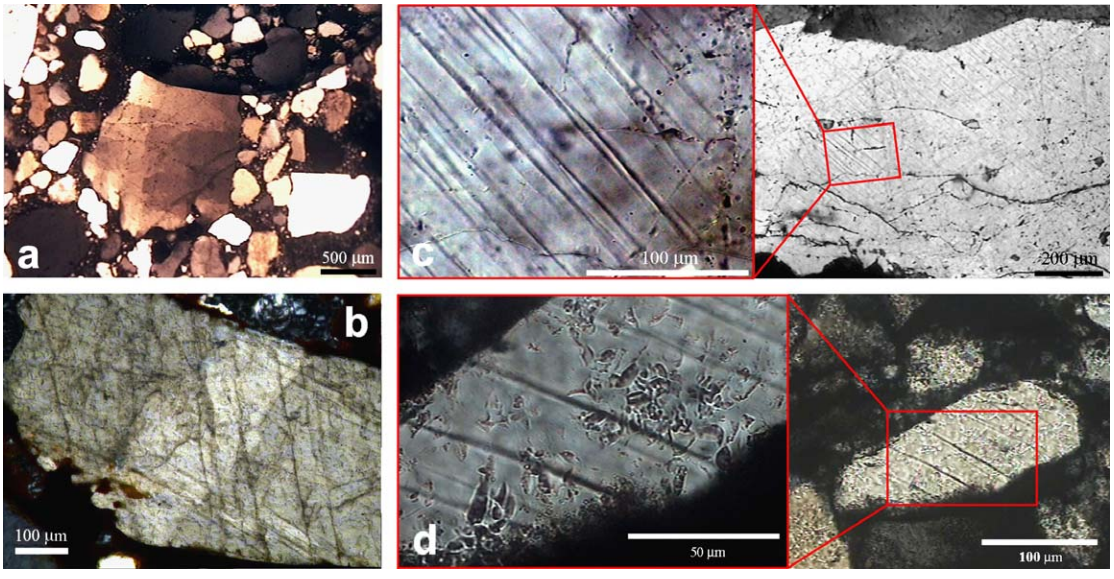

Fig. 16. Photomicrographs (crossed polars) of quartz grains in breccia and sandstone samples: (a) domain extinction in GKCF29, (b) sub-planar deformations associated to domain extinction in GKCF27, sub-planar micro-deformations in GKCF02 (c) and GKCF25 (d).

collected on the rims of several structures (cf. Table 1). Quartz is the predominant mineral component of all samples; minor components include phyllosilicates, iron oxides, and some accessory minerals such as zircon. Many quartz grain in these samples contain sub-planar micro-deformations. This includes domain extinction as shown in Fig. 16a, as well as relatively broad (250 µm) deformation bands. Fig. 16b shows a set of sub-planar deformations that resemble cleavage. Figs. 16c and d display sub-planar optical discontinuities reminiscent of planar fractures (PFs), known from weakly shocked quartz (1–8 GPa pressure range) of many impact structures (Stöffler and

Langenhorst, 1994; Grieve et al., 1996), but also strongly resembling tectonically induced deformation lamellae (Vernooij and Langenhorst, 2005). It must be noted that PFs by themselves are not directly impact-diagnostic, but where they occur in relative abundance, they may provide indication for the possible presence of an impact structure. In our samples, many of these features have been resolved as sub-planar open fractures. Their spacing is generally of the order of 5–20 μm, with many having spacing of about 10 μm. For samples containing such micro-deformations (cf. Table 1), we observed between 1 and 5 quartz grains with sub-planar optical discontinuities in the thin section, corresponding to abundances of 2000–10,000 weakly deformed quartz grains per m^2. In order to confirm if the observed micro-deformations are shock related, we shall have to measure their orientations with respect to the crystallographic axes and check that they are in the expected directions for shock features (Grieve et al., 1996). Further work, including TEM analysis, is required to help determine the origin of these features.

3.3. Ostracodes and fossil wood

We found a sample of chert in a sandstone outcrop in the northwestern part of GKCF21 (site 2a, cf. Fig. 6) that consists mainly of silicified ostracodes. The study of a polished surface and of thin sections shows that the sample represents a grainstone that was subsequently silicified. Each grain is composed of valves and carapaces of ostracodes (cf. Fig. 17). Such accumulations are known in recent deposits as ''ostracode sand lags'' (Cohen, 1987) and in fossil deposits as ''ostracodite'' or ''ostracode grainstone''. A characteristic feature in the thin sections is the common presence of imbricate valves. Similar imbrication of ostracode valves and carapaces is rather common in lacustrine sediments, and is referred to as ''nested valves'' (Sohn, 1979), ''cone in cone'' (Szczechura, 1971), ''plate stack,'' or ''stacked aggregates'' (Arp, 1995). Such a concentration of valves and carapaces most likely results from drying and thus secondary concentration of the fauna at a lake margin (concentrations reaching 6000 valves per gram sediment have been reported in maar lakes inside volcanic craters from southeastern Australia (De Deckker, 1982)). Numerous complete ostracodes and single valves have been extracted from the chert using diluted hydrofluoric acid: the shape and absence of differentiated hinge structures clearly indicate that we are dealing with a lacustrine genus of the Cyprididae family. In fact, this fauna is most likely mono-specific. The small size (0.8 mm) and the total absence of ornamented forms (reticulate, noded, spinose) that characterize pre-Tertiary non-marine ostracode faunas, strongly suggest a post-Cretaceous, albeit undifferentiated Cenozoic age. The shape and small size (<1 mm) of a few carapaces observed by electron miscroscopy (Fig. 17d)

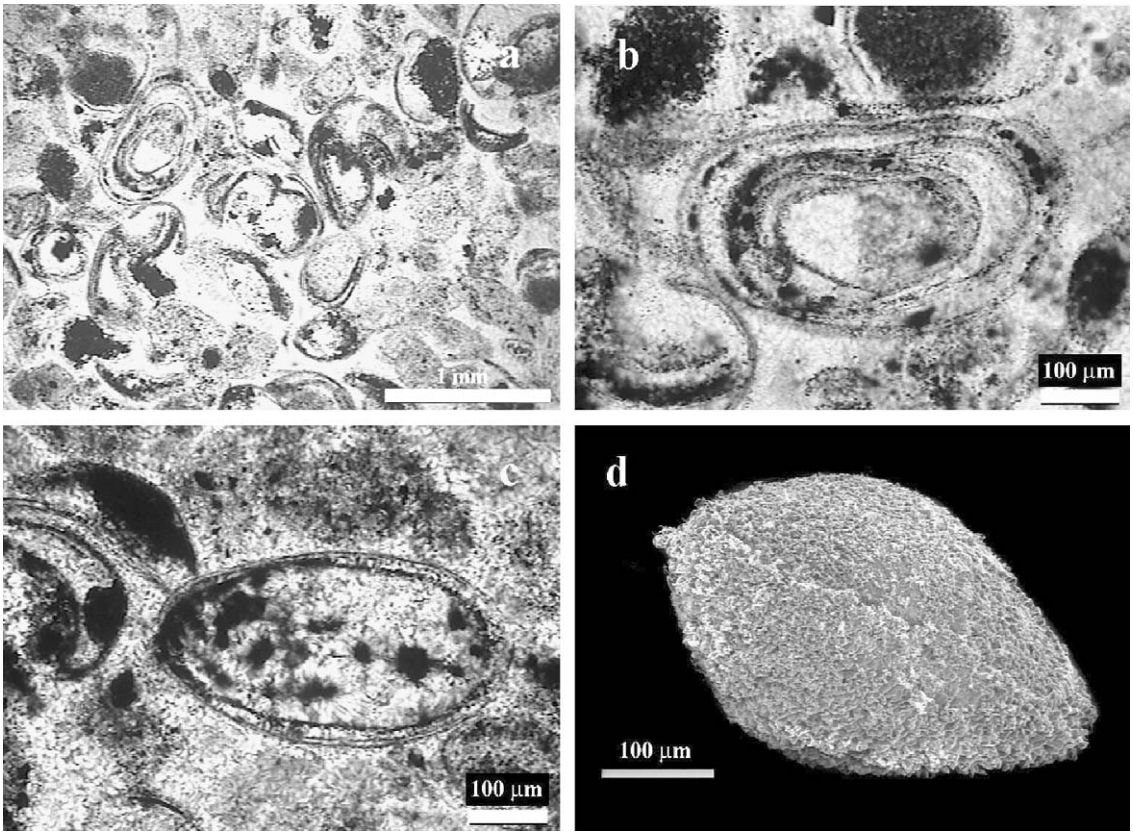

Fig. 17. Silicified ostracodes found in GKCF21: observed by optical (a–c) and electron (d) microscopy. Chert microfacies showing several ostracode sections (a), ostracode thin section showing stacked valves (b), ostracode longitudinal section showing the two valves (c).

suggest affinity to the genus *Cypridopsis*, which is no older than Oligocene. Lacustrine deposits with ostracodes are known from Miocene sediments of the impact crater lakes of Steinheim and Nördlinger Ries in southern Germany (Janz, 1995, 2000): in the Miocene of the Nördlinger Ries, high densities of valves and carapaces can be observed, forming ostracode-grainstones (Arp, 1995). These grainstones were deposited in association with algal bioherms in the eulittoral zone of the lake, the "stacked aggregates" of ostracode valves and carapaces being the result of an hydromechanical effect due to wave agitation. The sandstone outcrop in structure GKCF21 also yielded four pieces of silicified homoxylous wood of presumed conifer origin. These trees grew on the slopes inside the structure and have been fossilized in a swamp that occupied its lowest level. We can assume that the GKCF21 structure acted as a peculiar biotope in the past.

3.4. Ground-penetrating radar sounding

GPR soundings were performed on 10 of the visited structures (cf. Table 1) and on some flat areas between these structures, using an experimental high-gain pulse repetition ground-penetrating radar provided by Geophysical Survey Systems Inc. (Heggy and Paillou, 2006). The system was operated with a mid-frequency-range antenna configuration, covering a broad band from 150 to 400 MHz with a nominal central frequency of 270 MHz. A shielded antenna, with a net nominal radiated power output of 800 mW, was coupled to the surface during the data acquisition. Data acquisition was performed in continuous mode with constant offset in open areas in order to avoid surface clutter from in-range topography of the structure rims. We could map the subsurface down to 20 m depth, with a vertical resolution of a few tens of centimeters. The primary goal of the GPR investigations was to map shallow structural elements such as faulting, fractures and chaotic buried terrains. The collected data showed the occurrence of such features in the quasi totality of the radar transects. Significant lack of stratigraphy in the first 20 m of the subsurface is an important observation throughout the study area: chaotic disturbance of bedrock stratification is observed in the flat inter-structure areas, as shown in Fig. 18 (top) on a 300-m-long profile acquired close to GKCF13. We can clearly identify the perturbed and fractured bedrock (purple), which is covered by a few-meter-thick layer of aeolian deposits (yellow). In particular, we can observe scatterers with typical hyperbolic shape, a characteristic of diffraction mechanisms that rise in the presence of fractures and boulders of dimension comparable to the radar wavelength in the soil (Watts and England, 1976). Data migration suggests the entire observed diffraction patterns are the result of fracturing and breccia deposits. This interpretation agrees with the limited observations we made on the outcropping rims of several structures. Profiles in the flat inter-structure areas also revealed the presence of small buried bowl-shaped structures that do not outcrop at the surface. Fig. 18 (bottom) shows a 60-m-long radar profile that crosses GKCF28, a 40-m circular structure located in site 2a (cf. Fig. 6). We can clearly see the structure's curvature, its flat bottom at a depth of 4 m, about one-tenth of its diameter. Similar ratios have been observed for most of the structures covered by the GPR study. The GPR profile of Fig. 18 (bottom) also shows the structure fill of well and horizontally stratified aeolian deposits (yellow) and the fractured and brecciated

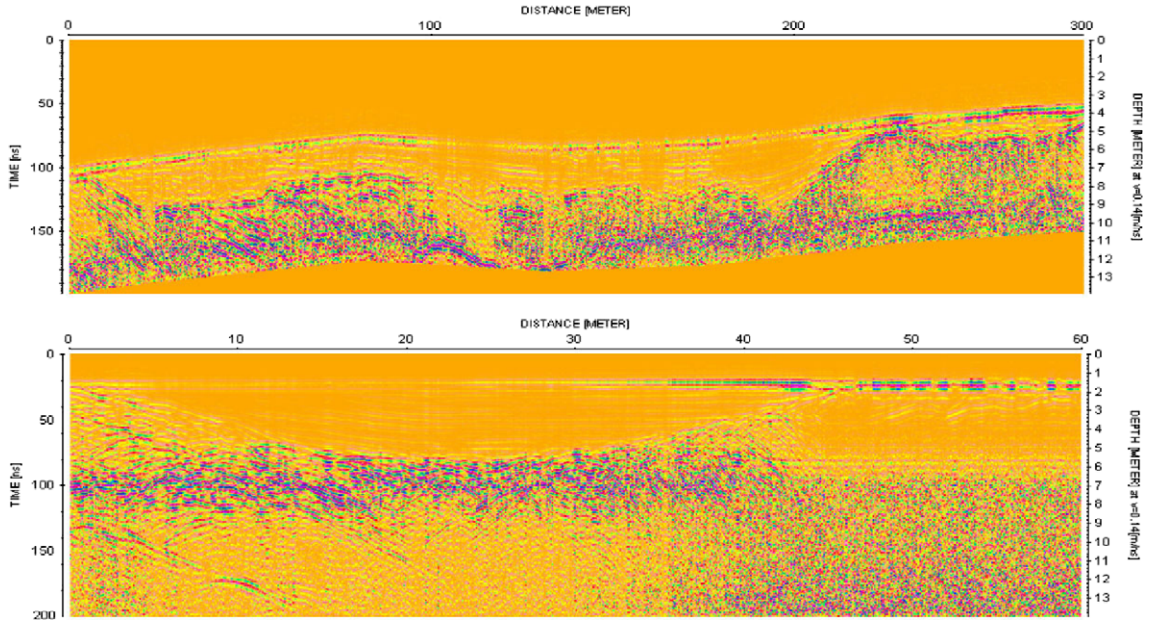

Fig. 18. Two 270 MHz GPR profiles showing subsurface structures. Top: a 300-m-long profile in a flat inter-structure area close to GKCF13 showing a perturbed and fractured bedrock covered by a few meters of aeolian deposits. Bottom: GPR cross-cut of structure GKCF28 (40 m in diameter), showing a clear paraboloid shape of perturbed bedrock buried under 4 m of aeolian deposits.

bedrock that diffuses the signal at the bottom of the structure, giving rise to the purple hyperbolic forms observed at 6 m depth. All GPR profiles obtained for the 10 sites reveal the same subsurface morphology: a perturbed paraboloid structure buried under sediments. In terms of lack of stratigraphy and scattering phenomena, they are quite different from GPR profiles observed for volcanic craters: for instance lava deposits do not exhibit such a chaotic structure (Heggy et al., 2006).

4. Discussion of the possible origin of the structures

4.1. Hydrothermal vent complexes

In large igneous provinces, such as the Siberian traps, the Karoo Province in South Africa, and the North Atlantic Volcanic Province, fluid seeps in volcanic sedimentary basins can produce extensive magmatic complexes: for example, more than 700 hydrothermal vent complexes spread over more than 85,000 km^2 have been observed in the More and Voring basins, offshore in the Norwegian Sea (Svensen et al., 2003). Eye-shaped structures were formed there as a consequence of magmatic sill emplacement during the late Paleocene: tips of transgressive sills produced vertical structures reaching the paleo-surface, where they terminate in eye-shaped structures. Vent complexes can range from almost purely volcanic in nature to those entirely filled by sedimentary materials. Typical vent structures present inward-dipping (up to 45°) sedimentary sequences surrounding a central complex with multiple sandstone or dolerite dykes and pipes, associated with hydrothermal breccias. Abundant sediment dykes cutting dolerite sills and large volumes of brecciated sediments have been observed in the Karoo basin in South Africa (Jamtveit et al., 2004). Vents there are generally eye-shaped, with a few circular structures. They are less than 2 km in diameter, with typical diameters on the order of hundreds of meters. A schematic evolution of hydrothermal vent complexes was proposed by Jamtveit et al. (2004): boiling of pore fluids hundreds of meters below the surface causes fluid pressure to build up. The fluid expulsion is associated with fragmentation and generation of hydrothermal breccias, and the erupted material forms crater rim deposits at the surface. Subsequently, large (several-meter-scale) pipes of fluidized material cross-cut the brecciated rocks, with smaller hydrothermal pipes forming during later reworking. Vents are spatially connected to the termination of sill intrusions deeper in the basin, as they represent conduits for overpressured fluids and fluidized sediments. Such structures, when formed by the intrusion of voluminous mantle-derived melt in carbon-rich sedimentary strata, may have caused a huge release of methane into Earth's atmosphere/ocean; this mechanism has been proposed as a possible explanation for the Early Eocene global warming stage (Svensen et al., 2004).

The typical size (about 150 m) and number (more than 1300) of the structures observed in the Gilf Kebir region are compatible with the hydrothermal vent hypothesis. An intruded area of 40,000 km^2 is also consistent with such sill intrusion, and the steep slopes of the rims of small structures that we observed in the field are compatible with conduit structures reaching the surface. The brecciated sediments we have found around most of the visited structures could have been produced by fluidized sediments reaching the surface. Also, the few basalt dykes that cross-cut some of the crater-like structures could be associated with a magmatic-hydrothermal process. In that scenario, the shatter-cone-like features we observed during fieldwork should be considered as the result of wind erosion.

However, southwestern Egypt is not known as part of a large igneous province. It is thus required to discover a major (and still unknown) hydrothermal event there that could have produced such vent complexes. The locally occurring alkali-olivine basalt dykes and volcanic craters observed indeed in the Gilf Kebir region have, until now, been related to the opening of the Rea Sea (Klitzsch and Schandelmeier, 1990) (however, this alkaline magmatism remains to be dated by more accurate techniques). Many of the structures observed on satellite images and in the field show a roughly circular shape (even if erosion and tectonics often deformed them), whereas hydrothermal vents are commonly eye-shaped. GPR sounding performed on several structures revealed a flat bottom covered by sedimentary deposits: hydrothermal vents should show tracks of a vertical structure, the conduit zone connecting to the tip of a sill intrusion. Also, we could not find evidence of sediment dykes and pipes in the 62 structures we visited, even though they should be abundant in the case of hydrothermal vents (Svensen et al., 2006) (but lots of structures are still to be explored). Finally, we did observe micro-deformations in quartz in some of the rocks sampled in the crater-like structures: such features have not yet been reported in the case of hydrothermal vents.

4.2. Meteorite impacts

An alternative to the hydrothermal hypothesis could be cratering as a consequence of meteorite impacts. The paraboloid morphology of the structures confirmed by GPR sounding, the observation of shatter-cone-like fracturing phenomena, the abundant occurrence of breccias, and the presence of micro-deformations in quartz grains could be indications of the presence of impact structures in the Gilf Kebir crater field.

If the discovered crater field was created by meteorite impacts, we can very roughly compute the equivalent size of a single impactor body using the pi-scaling law (Holsapple, 1993). We considered a target density of 3000 kg/m^3 (impact into rather dense rock) and an impact angle of 45° (the most probable one) for three different types of projectiles: a cometary body made of ice (density 1000 kg/m^3), an iron meteorite (density 8000 kg/m^3), and a porous rocky asteroid (density 1500 kg/m^3). As most of the observed craters are small, we can estimate that the impactors were greatly affected by the atmosphere, and we should then

Table 2
Main impact crater fields on Earth

Name	Location	Extent (km^2)	Crater number	Crater size (m)	Impactor	Age (yrs)	References
Campo del Cielo	Argentina	60	20	10–103	IA type	4000	Sanchez and Cassidy (1966), Cassidy and Renard (1996)
Rio Cuarto	Argentina	30	10	50–4000	Chondrite	<3500	Schultz et al. (1992, 1994, 2004)
Kaali	Estonia	1	9	5–110	Octahedrite	3700	Tiirmaa (1992), Tiirmaa and Czegka (1996), Rasmussen et al. (2000), Raukas et al. (2005)
Macha	Yakutia	10	5	60–300	Siderite	7300	Gurov and Gurova (1998)
Henbury	Australia	1.25	13	5–145	Siderite	4200	Alderman (1932), McColl (1990)
Sikhote Alin	Siberia	1.7	150	1–27	Siderite	58	Krinov (1974)
Morasko	Poland	2.5	8	5–100	Octahedrite	3500–5000	Korpikiewicz (1978), Stankowski (2001)
Odessa	USA	0.5	5	6–170	Octahedrite	?	Barringer (1967), Smith and Hodge (1997), Holliday et al. (2005)
Wabar	Saudi Arabia	0.8	4	17–100	Octahedrite	290	Holm (1962), Prescott et al. (2004)

consider their terminal velocity, taken around 1 km/s (this value can be higher, so we shall overestimate the mass of the impactors). For each of the 1312 structures, we computed a projectile size using the pi-scaling method [http://www.lpl.arizona.edu/tekton/crater.html]. We then summed up the 1312 "spherical" projectiles in order to obtain a "total equivalent spherical impactor". We obtained diameters of 2365 m for a cometary body, 973 m for an iron meteorite, and 1989 m for a porous rocky asteroid. In all cases, the impactor remains a rather small projectile with a diameter of less than 2.5 km. The impact of an object in this size-range is estimated to occur on timescales not greater than 3 Ma (Morbidelli et al., 2002).

"Classical" strewn fields on Earth result from meteorite showers that typically produce a few meter to kilometer-sized impact craters in a single event, covering at most a 100 sq.km. (Passey and Melosh, 1980). They are also generally young (less than 10,000 years old), as erosion removes such small structures in a very short time. Actually, numerical modeling of impact crater field formation indicates that the maximum aerodynamic separation of a single impactor during its passage through Earth's atmosphere is on the order of hundreds of meters (Cook et al., 2003): this explains why all the known impact strewn fields on Earth do not extend over more than 80 km^2 (cf. Table 2). Clearly, the dimensions and shape of the Gilf Kebir area are not compatible with the mechanism of single meteorite breakup. However, recent numerical simulations of large asteroid breakups have shown that rubble-pile asteroids, consisting of weak aggregates of gravel-sized to boulder-sized components held together by gravity, are produced by collisions that continuously take place in the asteroid belt (Michel et al., 2001, 2003). As most planet-crossing bodies likely are fragments of larger parent bodies that were disrupted in the asteroid belt, at least most of the kilometer-size asteroids should have a rubble-pile structure. Such asteroids can fragment when approaching a planet because of tidal forces, as occurred when the comet Shoemaker–Levy collided with Jupiter (Asphaug and Benz, 1994; Solem, 1994). This scenario has also been invoked to explain the existence of a steady-state population of well-separated binary and even triple systems in the Near-Earth-Object population (Richardson et al., 1998; Marchis et al., 2005). Such a rubble-pile asteroid could then break up into several fragments during a first pass close to the Earth-Moon system, and encounter the Earth during a second pass, each fragment being then again divided into smaller pieces by atmospheric breakup. Although some calculations would be needed to test this, the impact of all these fragments on the Earth's surface might result in an extended crater field covering several thousands of km^2.

5. Constraints on the age of formation for the structures

As the detected structures are mainly located in the Sabaya Formation of Albian age, and considering that (1) some of them are transected by basalt dykes of likely Middle Eocene age (46 Ma according to Meneisy (1990)) and (2) ostracode accumulations of post-Cretaceous age occur in GKCF21, we can assume that the formation of these structures certainly took place between the Albian and Lutetian ages, i.e. between 112 and 46 m.y. ago. Before proposing additional constrains on the age of the structures, we shall first summarize the geological history in southwestern Egypt during the Cretaceous and Paleogene periods (after Said, 1990a,b).

The Cretaceous period witnessed four transgressive cycles in Egypt. The Aptian, Cenomanian, and Coniacian cycles have seen shallow seas in the region between the Nubian and Kufra massifs. The passage between these massifs, changing position as they were eroded, was filled by marine and coastal sediments of intertidal, supratidal, estuarine, and swamp environments, alternating with alluvial sedimentation. The fourth transgression took place during the Campanian-Maastrichtian, when shallow open marine conditions were present over large parts of present-day Egypt. As the study area is located in the Sabaya Formation of Albian age, only the last three transgressive cycles of the Cretaceous period are of interest here. After pro-delta deposits had been accumulated during the Aptian time, the Albian saw a regressive phase during which the

sea retreated to the North. In the Western Desert, the sandstone of the Sabaya formation accumulated, consisting of medium- to coarse-grained fluvial sandstone interbedded with muddy paleo-soil horizons. During the Cenomanian, a major marine transgression covered most of western Egypt. It reached the southern part of the country in a seaway between the Nubian massif and the Kufra basin in the late Cenomanian, with a maximum for the Egyptian eustatic sea level reached 95 m.y. ago. An abrupt marine transgression flooded the Dakhla basin, covering the Gilf Kebir region, and produced the Maghrabi Formation, characterizing a tidal flat environment in an estuarine to lagoonal system. It has to be noted that extended paleo-soil formations separate the Maghrabi from the underlying Sabaya Formation. The region of interest then remained a positive area during the Turonian, the great estuary that was covering the Dakhla basin during Cenomanian having disappeared. The Coniacian transgressive phase brought the sea to the South as far as Nubia, but mainly in a region corresponding to the actual Nile basin, so that the surroundings of the Gilf Kebir remained positive. The Santonian corresponds to a regressive phase that did not affect the region of interest. The Campanian represents the third Cretaceous transgression, which mainly covered northern Egypt and did not reach the Gilf Kebir area. After a short regressive period during the Early Maastrichtian, the last Cretaceous transgression took place and covered large areas of Egypt; the sea became much deeper and shales were deposited in the South (corresponding to the lower Dakhla Formation). The Paleogene period began with a transgression that went across the southern borders of Egypt into northern Sudan, following the Nile basin through the Kharga region, with the maximum transgression occurring during the Late Paleocene. After the Paleocene, the sea retreated toward the North almost continuously except for short transgressive intervals that mainly affected northern Egypt. Sediments left by this transgression were modeled by the relief inherited from the late Cretaceous: the Gilf Kebir area remained positive and was not affected by the Paleogene transgressions.

If the crater-like structures were created by meteoritic impacts, we need to find a way to preserve so many (more than 1300) and such small (down to 10 m in diameter) structures from erosion until the present time: a fast sedimentary process that covered and protected the ''fresh'' structures shortly after their formation is then required. Considering the paleo-geographic evolution of Egypt during the Cretaceous and Paleogene periods combined with our field observations, the most likely age of the observed structures could then be Cenomanian. The tilted paleo-soil levels, which we observed on the rim of several structures, could correspond to the boundary between the Maghrabi and Sabaya Formations: the crater-shaped structures would then have been formed before the end of the Cenomanian. As discussed above, in order to preserve such small structures from erosion, a short time is constrained between their formation in the Sabaya sandstone and the covering by marine sediments: the structures should have then formed at the beginning of the large Cenomanian transgression, i.e., between 100 and 94 m.y. ago. They would have later been preserved from fluvial and coastal erosion during the Late Cretaceous and Paleogene, as southwestern Egypt remained positive during these periods. In the Early Miocene, the Gulf of Suez and the Red Sea were produced as a consequence of intense tectonics, which was terminated by the desiccation of the Mediterranean basin and the beginning of a long erosion period that shaped the current ''face'' of Egypt. The late intense aeolian erosion which took place during the Holocene finally recently exhumed the Gilf Kebir crater field.

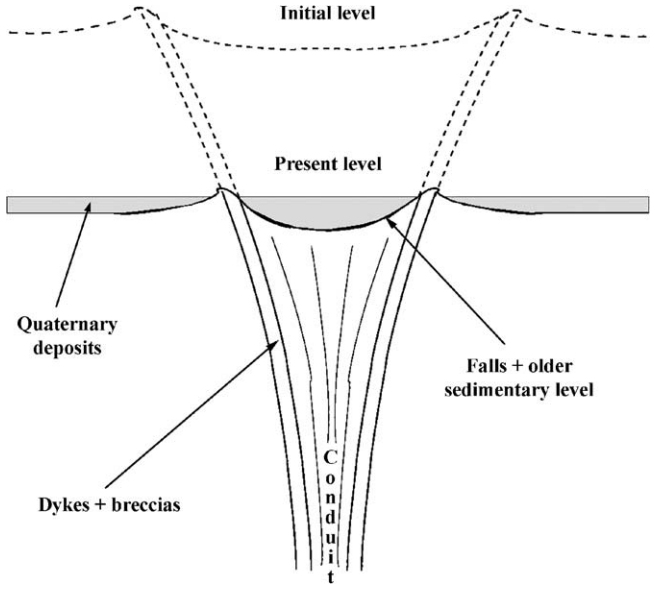

Fig. 19. Sketch of the result of erosion in the case of hydrothermal vents: the remaining structure at the surface is the outcrop of the vent conduit zone. The bottom of the surface structure would then be mainly constituted of sedimentary debris.

If the structures are hydrothermal vent complexes, preserving the surface terminating structures during millions of years is easier. In the hydrothermal hypothesis, the eye-shaped surface structures are spatially connected to the termination of sill intrusions, deeper in the basin. It means erosion will cut through the conduit zone, but it will always leave a smaller eye-shaped structure at the surface, as shown schematically in Fig. 19. In this case, the age of the structures remains relatively poorly constrained between 112 and 46 Ma.

6. Conclusion

We have presented results of two field exploration missions in the Gilf Kebir region in southwestern Egypt during 2004. We visited 62 crater-shaped structures among more than 1300 detected on satellite images, in an area covering more than 40,000 km^2. Considering the geological history of the region together with field observations, the formation of these structures certainly took place between the Albian and Lutetian ages, i.e. between 112 and 46 m.y. ago. The

good preservation of the structures could be due to the fact that they remained interstratified within the sedimentary section until recently. Two alternative hypotheses have been discussed to explain the origin of these structures: hydrothermal vent complexes, produced by fluid seeps in a volcanic-sedimentary basin, or the impact of numerous fragments generated in the break-up of a rubble-pile asteroid. At present, neither process fully satisfies the available observations but, whatever its origin, the Gilf Kebir crater field is of great scientific interest. Further field and laboratory studies are required in order to better understand the nature and origin of these structures.

Acknowledgements

The authors would like to thank JAXA/EORC, JPL, and the SPOT/ISIS/CNES program for providing satellite imagery, and they acknowledge GSSI and Exploration Instrument Inc. for providing the instrument support of the GPR survey. The authors are grateful to P.G. Eriksson, H.J. Melosh, P. Pinet, J. Plescia and to an anonymous reviewer for their critical and valuable comments on earlier versions of this manuscript. They are also grateful to A. Carion, E. Diemer, and F. Sahun for their participation in the fieldwork, to A. Barakat from EGSMA for his help, and to T. El-Mahdy from Dabuka Expeditions for organizing the logistics. This work was financially supported by the French ACI for Earth Observation and CNRS/INSU. E. Heggy was partially funded by NASA 2005 LPI-CAN. This paper is a Lunar and Planetary Institute contribution number 1311 and a University of the Witwatersrand Impact Cratering Research Group contribution number 101.

References

Alderman, A.R., 1932. The Henbury meteorite craters in Australia. Mineral. Mag. 23, 19–32.

Arp, G., 1995. Lacustrine bioherms, spring mounds, and marginal carbonates of the Ries-impact-crater (Miocene, southern Germany). Facies 33, 35–90.

Asphaug, E., Benz, W., 1994. Density of comet Shoemaker–Levy 9 deduced by modeling breakup of the parent rubble pile. Nature 370, 120–124.

Barakat, A., 1994. El-Baz crater: basaltic intrusion versus meteorite impact crater. In: Annals Of Geological Survey of Egypt, XXIV, pp. 167–177.

Baratoux, D., Melosh, H.J., 2003. The formation of shatter cones by shock wave interference during impacting. Earth Planet. Sci. Lett. 216, 43–54.

Barringer, B., 1967. Historical notes on the Odessa meteorite crater. Meteoritics 3, 161–168.

Cassidy, W.A., Renard, M.L., 1996. Discovering research value in the Campo del Cielo, Argentina, meteorite craters. Meteoritics Planet. Sci. 31, 433–448.

Clayton, P.A., 1933. The western side of the Gilf Kebir. Geogr. J. 81, 254–259.

Cohen, A.S., 1987. Fossil ostracodes from Lake Mobutu (Lake Albert): palaeoecologic and taphonomic implications. In: Palaeoecology of Africa and Surrounding Islands. Balkema, Rotterdam, pp. 271–281.

Cook, C.M., Melosh, H.J., Bottke, W.F., 2003. Doublet craters on Venus. Icarus 165, 90–100.

De Deckker, P., 1982. Holocene ostracods, other invertebrates and fish remains from cores of four maar lakes in southeastern Australia. Proc. R. Soc. Victoria 94, 183–220.

El-Baz, F., 1981. Circular feature among dunes of the Great Sand Sea, Egypt. Science 213, 439–440.

El-Baz, F., 1982. Crater forms in the Uweinat region. In: Desert Landforms of Southwest Egypt: a Basis for the Comparison with Mars, NASA Contract Memorandum CR-3611, pp. 79–89.

Grieve, R.A.F., Langenhorst, F., Stöffler, D., 1996. Shock metamorphism of quartz in nature and experiment: II. Significance in geoscience. Meteoritics Planet. Sci. 31, 6–35.

Gurov, E.P., Gurova, E.P., 1998. The group of Macha craters in western Yakutia. Planet. Space Sci. 46, 323–328.

Heggy, E., Paillou, Ph., 2006. Mapping structural elements of small buried craters using GPR in the southwestern Egyptian desert: implications for Mars shallow sounding. Geophys. Res. Lett. 33, L05202. doi:10.1029/2005GL024263.

Heggy, E., Clifford, S.M., Grimm, R.E., Dinwiddie, C.L., Wyrick, D.Y., Hill, B.E., 2006. Ground penetrating radar souding in mafic lava flows: assessing attenuation and scattering losses in Mars-analog volcanic terrains. J. Geophys. Res. 111, E6. doi:10.1029/2005JE002589.

Holliday, T., Kring, D.A., Mayer, J.H., Goble, R.J., 2005. Age and effects of the Odessa meteorite impact, western Texas, USA. Geology 33, 945–948.

Holm, D.A., 1962. New meteorite localities in the Rub'al Khali, Saudi Arabia. Am. J. Sci. 260, 303–309.

Holsapple, K.A., 1993. The scaling of impact processes in planetary sciences. Ann. Rev. Earth Planet. Sci. 21, 333–373.

Issawi, B., 1978. New finding on the geology of Uweinat Gilf Kebir, Western Desert, Egypt. Ann. Geol. Surv. Egypt 8, 275–293.

Jamtveit, B., Svensen, H., Podladchikov, Y.Y., Planke, S., 2004. Hydrothermal vent complexes associated with sill intrusions in sedimentary basins. In: Physical Geology of High-Level Magmatic Systems. Geological Society London Publications, pp. 233–241.

Janz, H., 1995. Neubeschreibung von *Strandesia risgoviensis* nov. com. (Crustacea, Ostracoda) aus dem Nördlinger Ries (Miozän, Süddeutschland). Stuttgarter Beiträge zur Naturkunde B 233, 1–13.

Janz, H., 2000. An example of intralacustrine evolution at an early stage: the freshwater ostracods in the Miocene crater lake of Steinheim (Germany). Hydrobiologia 419, 103–117.

Klitzsch, E., Schandelmeier, H., 1990. South Western Desert. In: Said, R. (Ed.), The Geology of Egypt. Balkema, Rotterdam, pp. 249–258.

Klitzsch, E., List, F.K., Pöhlmann, G., 1987. Geologic Map of Egypt 1:500000, Bir Misaha sheet, The Egyptian General Petroleum Corporation, Cairo, Egypt.

Koeberl, C., 2004. Remote sensing studies of impact craters: how to be sure? C. R. Acad. Sci. Paris Geosci. 336, 959–960.

Korpikiewicz, H., 1978. Meteoritic shower Morasko. Meteoritics 13, 311–326.

Krinov, E.L., 1974. Fragmentation of the Sikhote-Alin meteoritic body. Meteoritics 9, 255–262.

Lugli, S., Reimold, U.W., Koeberl, C., 2005. Silicified cone-in-cone structures from Erfoud (Marocco): a comparison with impact-genrated shatter cones. Impact Studies, vol. 6. Springer, Heidelberg, pp. 81–110.

Marchis, F., Descamps, P., Hestroffer, D., Berthier, J., 2005. Discovery of the triple asteroidal system 87 Sylvia. Nature 436, 822–824.

McCauley, J.F., Breed, C.S., El-Baz, F., Whitney, M.I., Grolier, M.J., Ward, A.W., 1979. Pitted and fluted rocks in the Western Desert of Egypt: viking comparisons. J. Geophys. Res. 84-B4, 8222–8232.

McColl, D., 1990. Distribution and sculpturing of iron meteorites from the major craters at Henbury. Meteoritics 25, 384–385.

McHone, J.F., Greeley, R., Williams, K.K., Blumberg, D.G., Kuzmin, R.O., 2002. Space shuttle observations of terrestrial impact structures using SIR-C and X-SAR radars. Meteoritics Planet. Sci. 37, 407–420.

Meneisy, M.Y., 1990. Vulcanicity. In: Said, R. (Ed.), The Geology of Egypt. Balkema, Rotterdam, pp. 157–174.

Meshref, W.M., 1990. Tectonic framework. In: Said, R. (Ed.), The Geology of Egypt. Balkema, Rotterdam, pp. 113–156.

Michel, P., Benz, W., Tanga, P., Richardson, D.C., 2001. Collisions and gravitational reaccumulation: Forming asteroid families and satellites. Science 294, 1696–1700.

Michel, P., Benz, W., Richardson, D.C., 2003. Fragmented parent bodies as the origin of asteroid families. Nature 421, 608–611.

Morbidelli, A., Jedicke, R., Bottke, W.F., Michel, P., Tedesco, E.F., 2002. From magnitudes to diameters: the albedo distribution of Near-Earth Objects and the Earth collision hazard. Icarus 158, 329–342.

Nicolaysen, L.O., Reimold, W.U., 1999. Vredefort shatter cones revisited. J. Geophys. Res. 104-B3, 4911–4930.

Paillou, Ph., Rosenqvist, A., Malézieux, J.-M., Reynard, B., Farr, T., Heggy, E., 2003a. Discovery of a double impact crater in Libya: the astrobleme of Arkenu. C. R. Acad. Sci. Paris Geosci. 335, 1059–1069.

Paillou, Ph., Rosenqvist, A., Farr, T., 2003b. A JERS-1 radar mosaic for subsurface geology mapping in East Sahara, In: Proc. IGARSS'03, Toulouse, France, July 2003, pp. 1493–1495.

Paillou, Ph., El Barkooky, A., Barakat, A., Malézieux, J.-M., Reynard, B., Dejax, J., Heggy, E., 2004. Discovery of the largest crater field on Earth in the Gilf Kebir region, Egypt. C. R. Acad. Sci. Paris Geosci. 336, 1491–1500.

Passey, Q.R., Melosh, H.J., 1980. Effects of atmospheric breakup on crater field formation. Icarus 42, 211–233.

Prescott, J.R., Robertson, G.B., Shoemaker, C., Shoemaker, E.M., Wynn, J., 2004. Luminescence dating of the Wabar meteorite craters, Saudi Arabia. J. Geophys. Res. 109. doi:10.1029/2003JE00213.

Rasmussen, K.L., Aaby, B., Gwozdz, R., 2000. The age of the Kaalijärv meteorite craters. Meteoritics Planet. Sci. 35, 1067–1971.

Raukas, A., Punning, J.M., Moora, T., Kestlane, U., Kraut, A., 2005. The structure and age of the Kaali Main crater, Island of Saarema, EstoniaImpact Studies, vol. 6. Springer, Heidelberg, pp. 341–355.

Richardson, D.C., Bottke, W.F., Love, S.G., 1998. Tidal distortion and disruption of Earth-crossing asteroids. Icarus 134, 47–76.

Roach, D.E., Fowler, A.D., Fyson, W.K., 1993. Fractal fingerprinting of joint and shatter-cone surfaces. Geology 21, 759–762.

Sagy, A., Reches, Z., Fineberg, J., 2002. Dynamic fracture by large extraterrestrial impacts as the origin of shatter cones. Nature 418, 310–313.

Sagy, A., Fineberg, J., Reches, Z., 2004. Shatter cones: branched, rapid fractures formed by shock impact. J. Geophys. Res. 109. doi:10.1029/2004JB00301.

Said, R., 1990a. Cretaceous paleogeographic maps. In: Said, R. (Ed.), The Geology of Egypt. Balkema, Rotterdam, pp. 439–450.

Said, R., 1990b. Cenozoic. In: Said, R. (Ed.), The Geology of Egypt. Balkema, Rotterdam, pp. 451–486.

Sanchez, J., Cassidy, W., 1966. A previously undescribed meteorite crater in Chile. J. Geophys. Res. 71, 4891–4895.

Sandford, K.S., 1935. The wadi hawa. Geogr. J. 85, 412–431.

Schultz, P.H., Grant, J., Collins, W., Lopez, J.P., Toselli, A.J., Castellanos, T.G., 1992. Rio Cuarto crater field. In: Lunar and Planetary Science XXIII, Houston, USA, pp. 1237–1238.

Schultz, P.H., Koeberl, C., Bunch, T., Grant, J., Collins, W., 1994. Ground truth for oblique impact processes: New insight from the Rio Cuarto, Argentina, crater field. Geology 22, 889–892.

Schultz, P.H., Zarate, M., Hames, B., Koeberl, C., Bunch, T., Storzer, D., Renne, P., Wittke, J., 2004. The Quaternary impact record from the Pampas, Argentina. Earth Planet. Sci. Lett. 219, 221–238.

Smith, T.R., Hodge, P.W., 1997. Discovery of impactite at the Odessa meteorite crater. Meteoritics Planet. Sci. 32, A122.

Sohn, I.G., 1979. Non marine ostracodes in the Lakota Formation (Lower Cretaceous) from South Dakota and Wyoming. Geol. Surv. Prof. Paper 1069, 1–22.

Solem, J.C., 1994. Density and size of comet Shoemaker–Levy 9 deduced from tidal breakup model. Nature 370, 349–351.

Stankowski, W.T., 2001. The geology and morphology of the natural reserve "Meteoryt Morasko". Planet. Space Sci. 49, 749–753.

Stöffler, D., Grieve, R.A.F., 1994. Classification and nomenclature of impact metamorphic rocks: a proposal to the IUSG sub-commission on the systematics of metamorphic rocks. Eur. Sci. Foundation Network Impact Cratering Newslett. 2, 8–15.

Stöffler, D., Langenhorst, F., 1994. Shock metamorphism of quartz in nature and experiment: I. Basic observation and theory. Meteoritics 29, 155–181.

Svensen, H., Planke, S., Jamtveit, B., Pedersen, T., 2003. Seep carbonate formation controlled by hydrothermal vent complexes: a case study from the Voring Basin, the Norwegian Sea. Geo-Mar Lett. 23, 351–358.

Svensen, H., Planke, S., Malthe-Sorenssen, A., Jamtveit, B., Myklebust, R., Rasmussen Eidem, T., Rey, S.S., 2004. Release of methane from a volcanic basin as a mechanism for initial Eocene global warming. Nature 429, 542–545.

Svensen, H., Jamtveit, B., Planke, S., Chevalier, L., 2006. Structure and evolution of hydrothermal vent complexes in the Karoo Basin, South Africa. J. Geol. Soc. London 163, 1–12.

Szczechura, K., 1971. Results of the Polish-Mongolian palaeontological expeditions. Part III. Freshwater ostracodes from the Paleocene of the Nemegt Basin, Gobi Desert, Mongolia. Palaeontol. Polonica 25, 85–97.

Tiirmaa, R., 1992. Kaali craters of Estonia and their meteoritic material. Meteoritics 27, 297–301.

Tiirmaa, R., Czegka, W., 1996. The Kaali crater field at Saaremaa (Osel), Estonia: geological investigations since 1827 and future perspectives. Meteoritics Planet. Sci. 31, A142.

Vernooij, M.G.C., Langenhorst, F., 2005. Experimental reproduction of tectonic deformation lamellae in quartz and comparison to shock-induced planar deformation features. Meteoritics Planet. Sci. 40, 1353–1361.

Watts, R.D., England, A.W., 1976. Radio-echo sounding of temperate glaciers: ice properties and sounder design criteria. J. Glaciol. 17, 39–48.